Daylight scattering by late antique window glass from Ephesus

Reconstructing the distribution of daylight in lost architecture

Lars O. GROBE, Lucerne University of Applied Sciences and Arts, Switzerland
Andreas NOBACK Technische Universität Darmstadt, Germany
Franziska LANG, Technische Universität Darmstadt, Germany
Luise SCHINTLMEISTER, University of Vienna, Austria
Helmut SCHWAIGER, Austrian Archaeological Institute, Austrian Academy of Sciences, Austria

Abstract: Starting from the 1st century CE, the availability of window glass throughout the Roman empire fosters the utilization of daylight in architecture. Due to features introduced by manufacturing, it affects the spatial distribution of daylight in buildings, and thereby the visual perception of architecture. Finds of window glass in the context of a mixed-use, residential house, located in a late-antique–medieval urban quarter in Ephesus, ask for a sound understanding of these immaterial aspects of architecture on the perception and utilization of buildings. The reconstruction of the building's illumination is challenging, since it has to replicate the effects of fenestration on admitted light, and therefore requires models of the light scattering by window glass. To prepare such a reconstruction attempt, two data-driven modelling techniques are evaluated. One is based on the direct characterization of light scattering by gonio-photometric measurements. The other technique employs ray-tracing on geometric surface models of the glass micro-structures, acquired by confocal microscopy, to derive effects on light scattering. The exemplary application of the techniques to an exemplary glass fragment from the site provides two models of the sample's scattering properties, including effects of corrosion and other alteration mechanisms. Both modelling techniques achieve qualitative accordance and demonstrate the applicability of the resulting models in daylight simulation. Quantitative differences between the two models indicate the importance to also account for effects by the glass volume and inclusions. The research lays the foundations for the planned modelling of glass based on replicated samples and processed finds, and shall ultimately lead to a plausible reconstruction of the building's illumination in late antiquity.

Introduction

Glass and daylight in late antique building

Since the advent of window glass, first used in Roman baths of the 1st century CE (Baatz, 1991) and soon applied in other public and private buildings, the availability of daylight in architectural spaces is inseparably intertwined with the practice of glassmaking (Foy and Fontaine, 2008; Michielin, 2019). Finds from numerous locations indicate that in late antiquity, window glass was readily available throughout the empire. Primary production of Natron glass appears to have been centralized close to the sources of raw materials in the Near East, and nourished the trade with glass chunks, that were then processed to secondary products such as window panes in workshops that were spread over the entire empire (Degryse et al., 2014). Since the end of the 2nd century CE, window glass was mainly produced from blown glass cylinders, that were cut, unfolded, and flattened to panes with typical sizes of 200 mm to 800 mm (Komp, 2009; Arletti et al., 2010). Despite the inclusion of bubbles in the glass volume, such panes are assumed to achieve a higher clarity than formed or crown glass due to their smooth surfaces (Grobe et al., 2019).

The chemical composition of glass, as well as the surface irregularities and inclusions that result from its artisanal processing (Komp, 2009) shape the spectral and spatial distribution of transmitted light, and thereby the visual perception of the illuminated interior (Noback et al., 2018). While the spectral composition of transmitted light mainly affects colour perception, scattering by the glass modulates the distribution of light in the attached architectural space and on its surfaces, and affects the appearance of the window panes that can allow a view to the outside in the case of clear glass, or lighten up and act as large area sources under direct sunlight in the case of diffuse scattering (Noback et al., 2017; Noback, 2019; Grobe et al., 2019). The resulting luminous environment is not static, but continuously changing with the external sky conditions and—in the case of direct sunlight—the solar geometry (Inanici, 2014).

Reconstruction and daylight simulation in historical science

The analysis and reconstruction of Roman and late antique interiors have a long tradition in building history (Demetrescu et al., 2016). Studies of daylighting in this context are however rare and often depend on assumptions in lack of empirical data (Papadopoulos and Earl, 2014). Computational simulation of light propagation in three-dimensional models is employed in building design and optimization (Ochoa, 2012; Jones, 2017), but can also be applied to evaluate the illumination of lost, reconstructed architecture (Grobe et al., 2010; Devlin, 2012; Earl et al., 2013; Papadopoulos and Earl, 2014; Happa et al., 2012).

Measurement and modelling of the optical properties of window glass are key elements of such simulations, if daylight is the primary source for illumination, and bridge a gap between material culture and sensory studies (Noback, 2019). Models of the effect on the spectral composition of transmitted light have been developed and applied in historical sciences (Cerise et al., 2012; Thanikachalam et al., 2016). Only few attempts to replicate scattering by surface irregularities and inclusions as characteristic for historic glass, as well as translucent tiles, have been made, that typically rely on simplified measurement and modelling techniques (Patay-Horvárth, 2016). This is contrasted by the rapid development of characterization (Apian-Bennewitz, 2014) and modelling techniques

(Ward et al., 2014; Lee et al., 2018) in the field of building science, that support the development and application of optically complex fenestration addressing an increasing demand for comfort and energy efficiency (Kuhn, 2017). Advanced measures of the spatial distribution of daylight in buildings, the gonio-photometric characterization of scattering by fenestration, and its modelling in daylight simulation have just recently been demonstrated in few, targeted studies (Monteoliva et al., 2019; Grobe et al., 2019; Noback et al., 2017).

Challenges in the modelling of Roman window glass

Transmission through modern, clear float-glass can be modelled either by Fresnel equations as a function of the incident direction (θ_i), and the index of refraction and absorptance of the glass substrate, or by fitting polynomials to transmission measurements to account for the effects of coatings and multiple panes in modern fenestration (Karlsson, 2000). While any such perfectly clear glass has the property that the direction of light is not changed by transmission if both surfaces of the pane are coplanar, Roman window glass features surface irregularities and inclusions in the substrate that cause scattering, e.g. the deflection of transmitted light. Gonio-photometers acquire this spatial modulation of light, that is described by the "Bidirectional Scattering Distribution Function" (BSDF) (Heckbert, 1991; Stover, 2012) as the light transport through a specimen for any pair of incident and outgoing, scattered directions ($\theta_i, \phi_i, \theta_s, \phi_s$). The BSDF is implicitly defined by the Rendering Equation (Kajiya, 1986) and relates incident (L_i) to scattered (L_s) radiance:

$$L_s(\theta_i, \phi_i, \theta_s, \phi_s) = \int_{\theta_i, \phi_i}^{\omega_i = 4\pi} BSDF(\theta_i, \phi_i, \theta_s, \phi_s) \times L_i(\theta_s, \phi_s) \times \cos\theta_i \, d\omega_i$$

Numerous models of the function exist that allow for fitting to measured BSDF data, or that can be parametrized based on few, established optical measurements or by known, physical meaningful properties such as e.g. surface roughness (Walter, 2007; Dai et al., 2009; De Rousiers et al., 2011). The lighting simulation software RADIANCE models translucency by applying the Ward reflection model (Geisler-Moroder and Dür, 2010) to transmission. This model has been employed in the modelling of Roman window glass, but is of limited generality since it represents directional transmission by a Gaussian peak based on a surface roughness parameter that is independent of the incident direction (Noback et al., 2018).

Data-driven modelling addresses this limitation and approximates arbitrary BSDFs by interpolation between discrete values (Ward et al., 2014). To achieve high directional resolution with compact representations, compression such as wavelet transforms (Wu et al., 2019), and reduction algorithms generating models of adaptive resolutions (Ward et al., 2012) are employed. The latter has been implemented in RADIANCE and is commonly referred to as the tensor tree model, due to the hierarchical data-structure that results from merging elements of an initial tensor that represent adjacent regions where the slope of the BSDF is low.

The properties of archaeological finds are not identical to those of window glass when it was in use. The characteristics of the sample rather form a convolution of its original properties, caused e.g. by glass composition and glass-making techniques, and later deterioration, caused e.g. by corrosion and contamination. Even a perfect model of the archaeological find therefore does not replicate the

effects of window glass in its original condition on the illumination of a building. Reconstruction of the latter consequently requires both,

- a general and accurate model of irregular scattering, and

- the elimination of the effects of corrosion and other deterioration mechanisms in the simulation.

We hypothesise that the primary cause of light scattering on Roman window glass is the structure of its surface. Two approaches are currently being evaluated by the authors to isolate deterioration of the glass, and to reconstruct its original light scattering properties: The temporary "healing" of surface defects by sealing small-scale cavities, and the replication of Roman window-glass by means of experimental archaeology. Application of either method would then allow to reconstruct the light scattering properties of the sample in its original condition by data-driven BSDF models, that can be generated directly from gonio-photometric measurements, or deduced by ray-tracing on the acquired micro-geometry of the surfaces.

Objectives

Aiming at a systematic research on the optical properties of Roman window glass of different origins, times and production methods as well as their impact on the development of fenestration, use and architectural typology, we describe the first outcomes of the development of modelling methods:

Testing our hypothesis, that light scattering is caused by the surfaces and hardly affected by the glass volume,

the development of data-driven transmission models by direct measurement of light scattering, and by the acquisition of the surface geometry and ray-tracing, and

the exemplary application of the resulting data-driven BSDF models in daylight in daylight simulation.

The elimination of deterioration effects, e.g. by the experimental replication of samples, or the proposed healing of surface defects, have not been covered yet.

Late antique window glass in a mixed-use house in Ephesus

Mixed-use houses in a late-antique–medieval urban quarter

A series of earthquakes in the 3rd century CE caused a sudden end to the heyday of Roman Imperial Ephesus. It took until the mid of the 4th century CE that reconstruction work has been undertaken (Ladstätter, 2019, p. 21). In the course of these measures, the lower city developed into the new religious and political centre of the late antique provincial capital: along with the construction of large public buildings, both profane and sacred in nature (Ladstätter, 2019, pp. 28–29), also the establishment of private residential quarters in the area of the former harbour gymnasium and the adjacent square—the so-called Halls of Verulanus—took place. A part of this residential area has been unearthed from 2011 until 2018 (Fig. a,b) and showed a series of three independent houses differing in size and decoration (Schwaiger et al., 2020). They are located right south of the bishop's church (Church of Mary) along a street which is accompanied by a portico. The buildings have been erected by the end of the 4th / beginning of the 5th century CE and have been in use until the second half of the 7th century CE, when they were destroyed by fire. The westernmost house and the one in the middle resemble imperial courtyard houses, whereas the easternmost house has a courtyard without

a   *b*   *c*
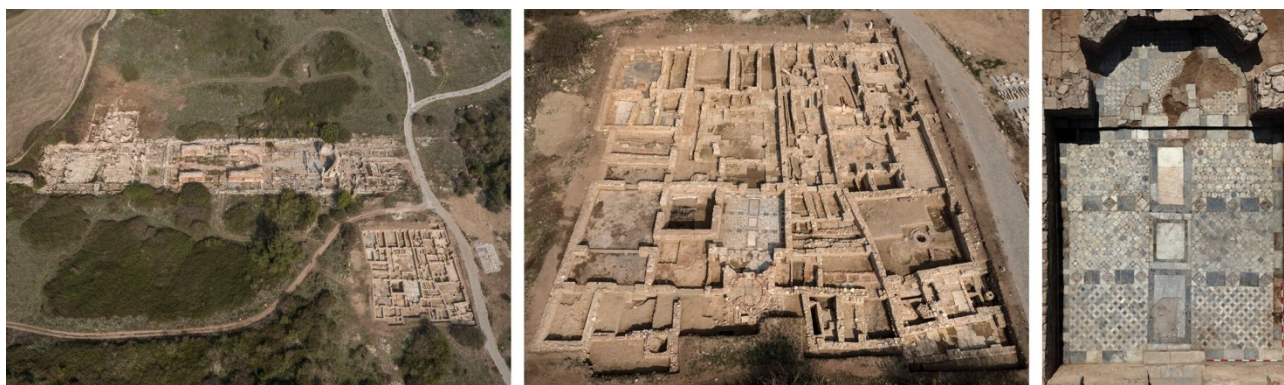
Fig. 1. Three excavated houses (a, b), marble floor in the largest house in the west (c). (© Niki Gail, ÖAI / ÖAW).

columns. Via entrances to the north, one could access the courtyards located in the inner of the house, which served as places of communication and dividers. Rooms grouped around these central spaces are differing in function and equipment. The rooms closer to the street in the north show clearly that they have been used for commercial and manufacturing purposes (Schwaiger et al., 2020). Especially the largest house in the west shows a series of representative rooms in the south (Fig. 1c, 1.16–1. 20 in Fig. 2). They show a lavishly decorated interior with mosaic and marble floors as well as the remains of wall paintings imitating marble revetments. In addition, the finds recovered from these rooms clearly identify them as spaces serving for representative needs of the house owner.

Since the house has not been abandoned but suffered severe destruction while being in use, all the inventory is preserved inside the rooms. In addition, elements of furnishing like the remains of doors, decorated beams and even window panes have been found. Hence, the whole furnishing and inventory remained within the destruction layers.

The glass finds

Large amounts of window pane fragments were found in house 1, the largest of the three units with an area of 764.70 m^2, located in the west of the urban quarter. The majority of the fragments is in a very good state of preservation and was unearthed primarily along the walls of richer, more prestigious rooms of house 1 (Fig. 2). Several almost completely preserved window panes have dimensions of around 150 mm×210 mm. The fragments were made of yellow-brown or green coloured glass with a thickness varying from 1.5 mm to 5.0 mm.

Of the various known techniques for the production of Roman window glass (Haevernick, 1981a; 1981b; Von Saldern, 1980, p. 91; 2004, p. 201; Baatz, 1991; Kanyak, 2009), two could be attributed to the finds. Almost all the panes are cylinder-blown. These finds are shiny on both sides, show a slightly streaky surface and elongated air bubbles. Three fragments are of the "matt-glossy type" with characteristics of casting. They feature one rough surface and they are also very thick compared to cylinder-blown glass. One such fragment shows the trace of a tool (imprint of a pair of pliers), used to stretch the corner of the pane.

A total of 5273 fragments were classified into colour groups and weighed (total weight: 27.96 kg, Fig. 3). The yellow and brown coloured pieces make up 53 % of the total weight and 39 % of the total

number of fragments. The green and aqua coloured fragments make up 41 % of the total weight and 49 % of the total number of fragments. Since glass breaks very easily, both very small (10 mm to 20 mm) and larger fragments (100 mm to 150 mm) are present. The state of preservation of the fragments varies greatly. Glass layers of 3 mm to 4 mm peel off the surface of pieces that are strongly affected by weathering. Thus, we cannot expect that the original state of the surface and the thickness of the fragment have been preserved.

It is still unclear how the window panes were installed. Frames could have been made of wood or marble as excavated in the Vedius Gymnasium (La Torre, 2008, p. 286) or the panes were placed in the moist mortar. Bronze frames with glass panes are known from the baths near the forum in Pompeii (Mau, 1899, p. 199).

Fig. 2. Density of window glass finds overlaid on the plan of house 1 (© Katharina Sahm, Luise Schintlmeister).
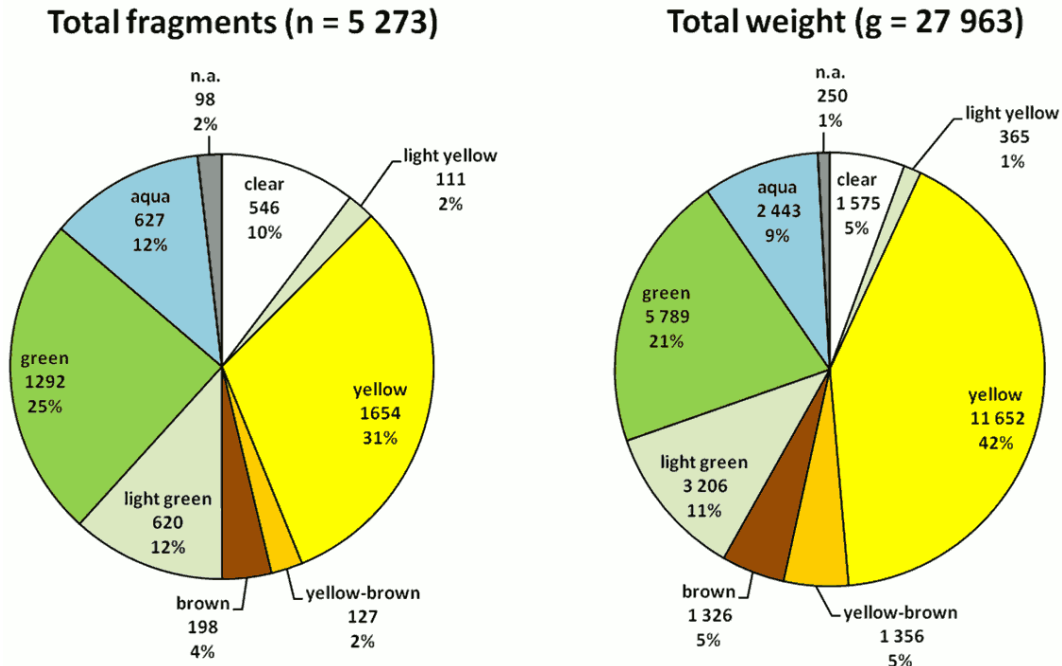
Fig. 3. Frequency and fraction of glass finds of different colours in house 1.

Sample and data-driven modelling methods

Two data-driven models of the sample's light scattering properties are developed from the gonio-photometric measurement of the BSDF, and from the surface geometry acquired by confocal microscopy.

An exemplary sample of late antique window glass

One sample was selected from the glass finds for a detailed characterisation, and to develop and test methods to model its light scattering properties as described in the subsequent sections. Consequently, this research does not provide a representative model for all the different fragments of window glass found in the site, but aims at testing methods for the characterization and modelling of late antique window glass.

The selected specimen is of approximate dimensions 70 mm×50 mm×3 mm (Fig. 10 a). Characteristic for the cylinder-blown type are its two flat and rather smooth surfaces, illustrated by the pronounced contrast that allows to read a text seen through the sample when it is placed directly on top of a printed sheet. Microscopic structures, that cover different regions of the surfaces at varying degree, cause diffuse scattering and are attributed to deterioration effects due to their non-uniform of the sample that appears to follow the curved longer edges and not the shorter, one of which is straight and may be a section of the original window-panes edge. A closer view reveals iridescence, a typical effect of laminar decomposition mechanisms that are caused e.g. by corrosion. The yellowish tint of the glass is assumed to be an original feature due to the chemical composition of the bulk material. The overall condition of the sample, compared to other exemplars of the collection, is considered good.

Modelling light scattering based on gonio-photometric measurements

Light scattering by the sample was directly measured by means of the BSDF. A scanning gonio-photometer was employed (Fig. 4), that acquires the distributions of scattered light by varying the directions of an illuminating light source and a detector relative to the sample by mechanical movement (Apian-Bennewitz, 2010). To ensure that the projected beam diameter on the sample does not exceed the specimen's width under oblique illumination by a stabilized 4 mW laser source with a peak wavelength at $\approx$ 520 nm, located between the maxima of human photopic ($\approx$ 555 nm) and scotopic ($\approx$ 505 nm) response, was employed in the measurement. The measurement is performed relative to a prior characterization of the illuminating beam rather than relying on a prior calibration.
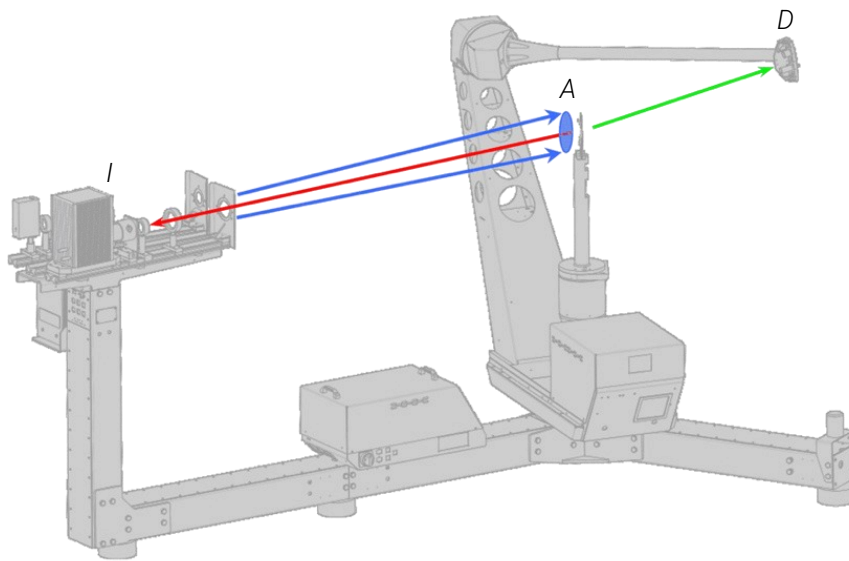
Fig. 4. Scanning gonio-photometer. Light scattered from the sample region A (blue), illuminated by illuminator I from incident direction θ_i, ϕ_i (red), is recorded by detector D at outgoing direction θ_s, ϕ_s (green) during its continuous movement on a configurable scan path. Illustration (Grobe, 2018) based on image © Peter Apian-Bennewitz.

| a | b | c |
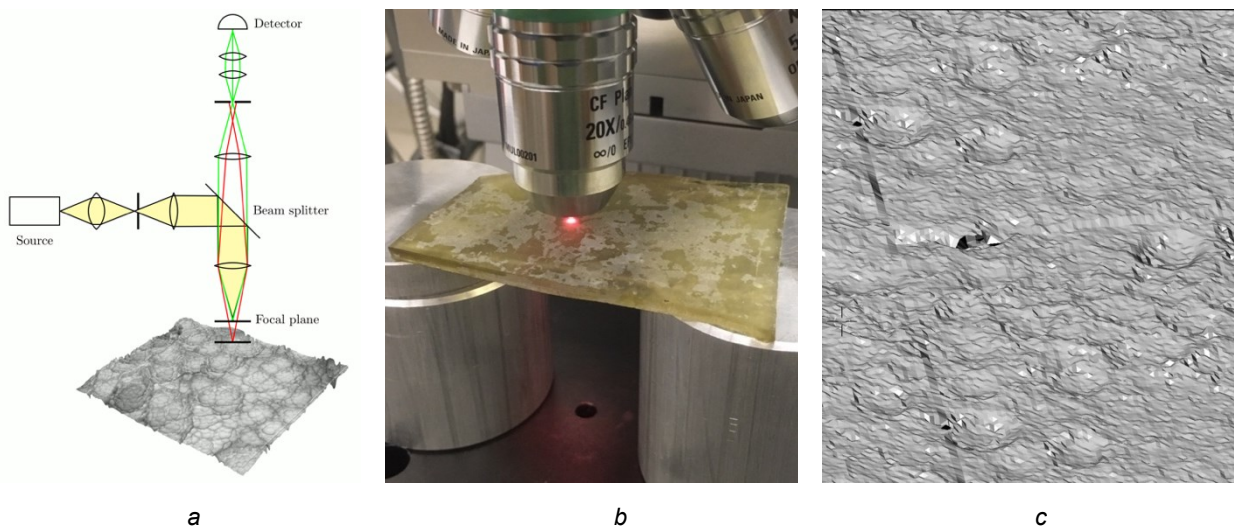
Fig. 5. Design principle of a confocal microscope (a), sample during acquisition of its surface geometry (b), and resulting, triangulated surface relief (c, all surface properties were set to opaque for illustration).

The sequential measurement of the BSDF allows to adapt its spatial resolution, allowing to e.g. refine peak regions, and covers a dynamic range that accounts for distinct specular peaks as well as the background of straylight by diffuse scattering. Assuming isotropic transmission, the hemispherical distribution of transmitted light was recorded in terms of illuminance at a dense set of > 150,000 arbitrary outgoing, or scattered, directions (θ_s, ϕ_s) for few incident directions defined by varying off-normal angle (θ_i) but constant angle (ϕ_i) in the sample plane. The coordinate system is relative to the sample.

The measured BSDF was exported as one tabular data-set per incident direction, with data-columns θ_s, ϕ_s and the corresponding value of the "Differential Scattering Function" (DSF), which is equivalent to the BSDF but stable at directions close to grazing (ASTM International, 2019):

$$DSF(\theta_i, \phi_i, \theta_s, \phi_s) = BSDF(\theta_i, \phi_i, \theta_s, \phi_s) \times \cos\theta_s$$

Employing a tool-chain implemented in RADIANCE, a transmission model was prepared by interpolation between the distributions of scattered light for the sparse set of measured, incident directions. First, the command pabopto2bsdf approximates the distributions by a set of Gaussian "Radial Basis Functions" (RBFs), and interpolates between the measured incident directions by variation of the basis functions' parametrizations. The command bsdf2ttree then samples the interpolants at discrete resolution and builds a three-dimensional tensor. This data-cube is subsequently translated into a tree-structure by selectively merging cells where the distribution's gradient is low. The result is a compact model, later on referred to as *Model M*, of locally adaptive resolution. Since directional scattering cannot be reliably extrapolated, *Model M* is valid only in the range of measured directions $\theta_i \leq 82.5°$ and returns just the diffuse background for incident directions close to grazing.

Acquisition of surface micro-geometry and ray-tracing to model light scattering

Light scattering by the sample, which comprises a theoretically clear, non-scattering material, is caused by refraction at the rough surfaces, which optically form the outer interfaces between a dielectric solid and air as its surrounding medium, and inclusions of air and other particles, that form internal interfaces. Employing confocal microscopy, the height reliefs of parts of the sample's front and back surfaces were prepared (Fig. 5 a and b). This should allow to relate the causal, geometric properties of the sample to its effective, optical light scattering properties.

Based on the acquired surface geometries, a second data-driven transmission model was generated. The front- and back-surfaces of the sample were tiled and arranged so that they, together with added side-surfaces, form a closed volume. All surfaces were attributed the optical properties of clear glass (refractive index 1.52). Note that this model does not account for volume scattering e.g. by bubbles or other impurities
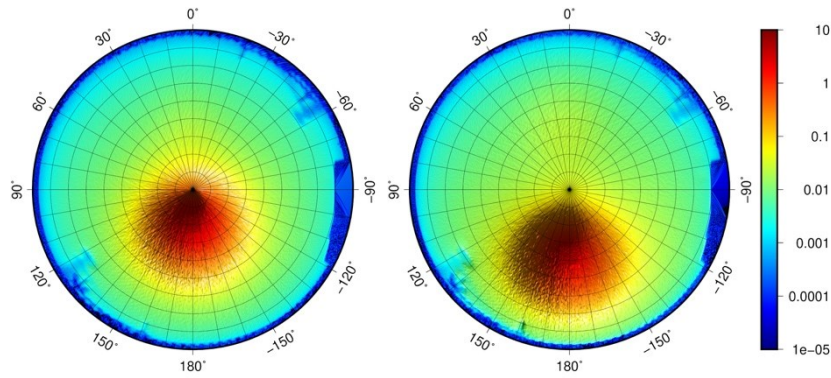
Fig. 6. Measured DSF for incident direction θ_i = 20° (a) and 40° (b), ϕ_i = 0°.

in the glass. Fig. 5 c illustrates the geometric model with opaque properties to increase readability of the surface structure.

The RADIANCE command genBSDF applies backward ray-tracing to the geometric model to solve light propagation through the sample. Adaptive data-reduction produces a computationally gener-ated, data-driven BSDF model in analogy to the measurement-based model generation process. Other than the latter, its computational counterpart provides *Model C* that is valid for any pair of incident and outgoing directions including those close to grazing.

Exemplary application of the models

To test the applicability of *Model M* and *Model C*, they are applied in an exemplary daylight simulation of a simplified room exposed to a sunny sky. The room model features a window of dimensions 0.80 m×1.10 m, that corresponds to a window in a villa in Pompeii (Spinazzola, 1953). Its panes are modelled as flat polygons of type BSDF in RADIANCE. All other surfaces are assumed to be opaque (reflectivity 0.70 for ceiling and wall, and 0.15 for floor and frames), and to scatter light as ideal Lambertian diffusers.

Two simulations are performed, one for each data-driven model[1]. The sun direction is orthogonal to the window-wall at an elevation of 75°. The simulation results in imagery with pixel values represent-ing—after conversion from radiometric to photometric units—luminance L [cd/m2]. The luminance maps are illustrated by the application of a colour scale. In addition, illuminance E [lx] was measured for selected locations on window, wall, floor and ceiling.

Results and discussion

Measured light scattering

The measured transmission distribution for two exemplary incident direction ($\theta_i = 20°$ and $40°$, $\phi_i = 0°$) is illustrated by Fig. 6. For all measured incident directions, distinct forward-scattering is observed that produces a widened peak in the hemispherical distribution. The transmitted peak is, as expected for glass with arbitrary perturbations, centred around the opposite of the incident

---

[1] Simulations were performed using the RADIANCE command rtpict with following parameters: -ss 32 (specular samples), -aa .1 (ambient accuracy), -ab 4 (ambient bounces), -ad 8192 (ambient divisions), -as 4096 (ambient super-samples), and -lw 1e-5 (limit weight).

a   *b*
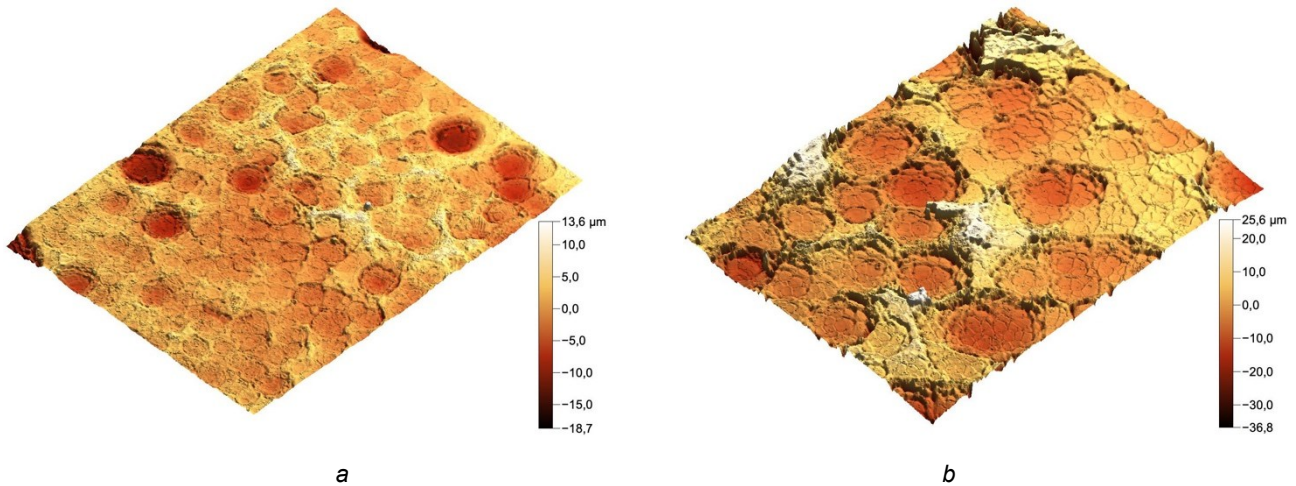
Fig. 7. Height maps of front (a) and back (b) surfaces, acquired under monochromatic illumination by a red laser.

direction. A region close to the sample horizon at $\phi \approx -90°$ is shaded by the vertical column holding

a   *b*
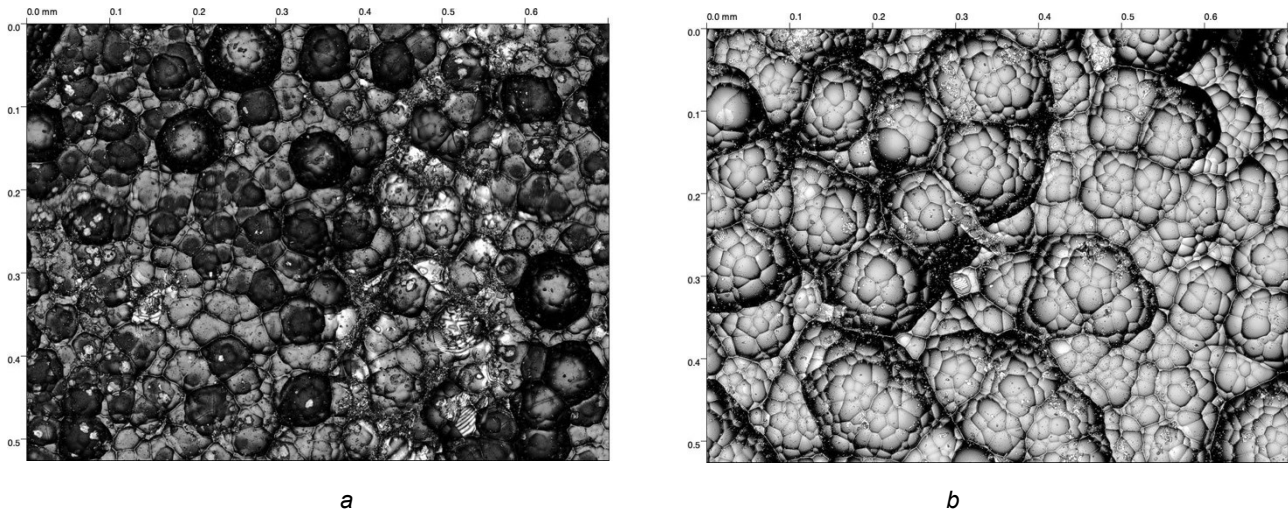
Fig. 8. Luminance maps of front (a) and back (b) surfaces, acquired under white illumination.

the sample mount, and appears black in the plot. Note that the logarithmic scale, covering five decades, compresses the peak and exaggerates the background.

Direct-hemispherical transmission τ_{d-h} was calculated by integration of the hemispherical distributions over all scattered directions (Table 1). Reaching 0.697 under normal illumination ($\theta_i = 0°$), it decreases with increasing obliqueness of the incident direction to 0.158 ($\theta_i = 82.5°$). Results of the gonio-photometric characterisation are available as a digital data-set (Grobe and Noback, 2019).

Surface micro-geometry of the sample

Confocal microscopy on the front and back surfaces provided two data-sets. The first data-set encodes the z-position of the focus where the pixel brightness reached its maximum, and thereby provides a height map of each surface. It is acquired under the monochromatic illumination of a red laser diode. Fig. 7 shows the reliefs of the front (a) and back (b) surfaces, with a colour map applied to the z-values. The recorded pixel elevations of the back surface cover a range of $\approx 60~\mu m$, while

those on the frontside are limited to $\approx 30\ \mu m$. A pattern of calderas covers the entire front and back surfaces. The surfaces within these calderas, especially on the backside, appear to be rough.

θ_l		0.0°	20.0°	40.0°	60.0°	82.5°
	measured	0.697	0.676	0.579	0.410	0.158
$\tau_{d\text{-}h}$	Model M	0.715	0.704	0.590	0.417	0.137
	Model C	0.860	0.835	0.713	0.497	0.266

Table 1. Measured and modelled direct-hemispherical transmission as function of the incident off-normal angle θ_l.

a   b   c
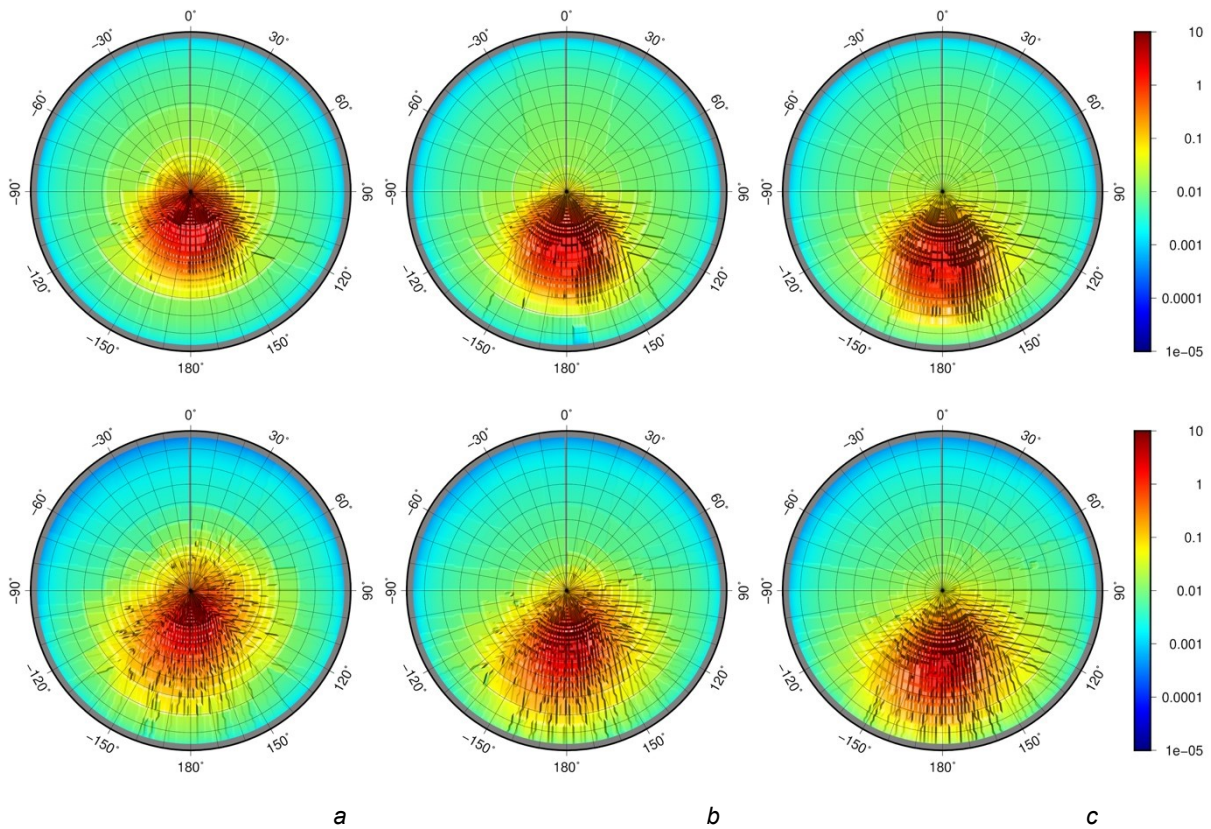
Fig. 9. Plots of the DSF from Model M (top) and Model C (bottom), θ_l = 20° (a), 30° (b), and 40° (c).

a   b   c
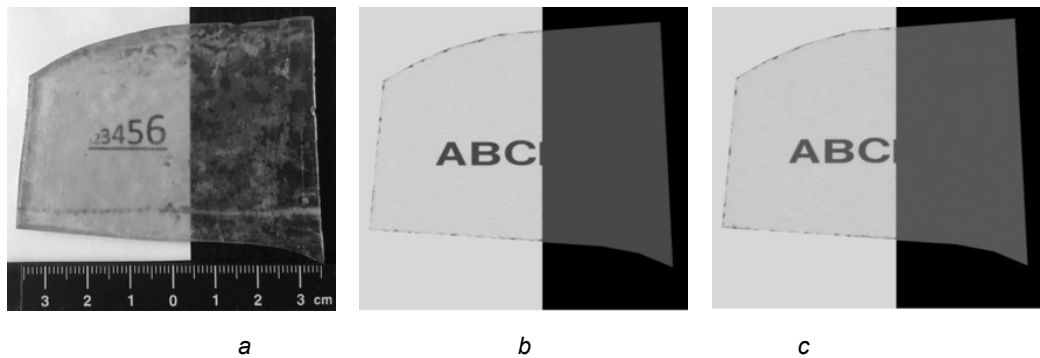
Fig. 10. Photograph of the sample, (a) and synthetic imagery by Model M (b) and Model C (c).

The second data-set, acquired under the illumination of a white light source, is a magnified image of the covered surface area where each pixel represents luminance as recorded so that the focus was

set according to the local elevation of the surface. The resulting, sharp imagery of Fig. 8 illustrates the geometric features of the sample's front (a) and back (b) surfaces at higher resolution than the height maps.

The relief of the backside reveals a structure of clustered craters. Small secondary pits cover the entire surface and follow the surface of larger, primary calderas, causing the apparent roughness observed on the height maps. This is contrasted by the frontside, where calderas of moderate diameter are the predominant characteristic. The secondary pits are not clearly identified on the frontside.

Caldera-like structures are typical for a glass degradation mechanism referred to as pitting in literature. One possible explanation for the two types of pits on the backside could be a change of the environmental conditions affecting the backside during the process, that did not occur on the front. However, this explanation attempt is a mere hypothesis that asks for further investigation. Regardless its causes, the effective perturbation of the surface can be assumed to have a strong influence on the light scattering properties of the sample.
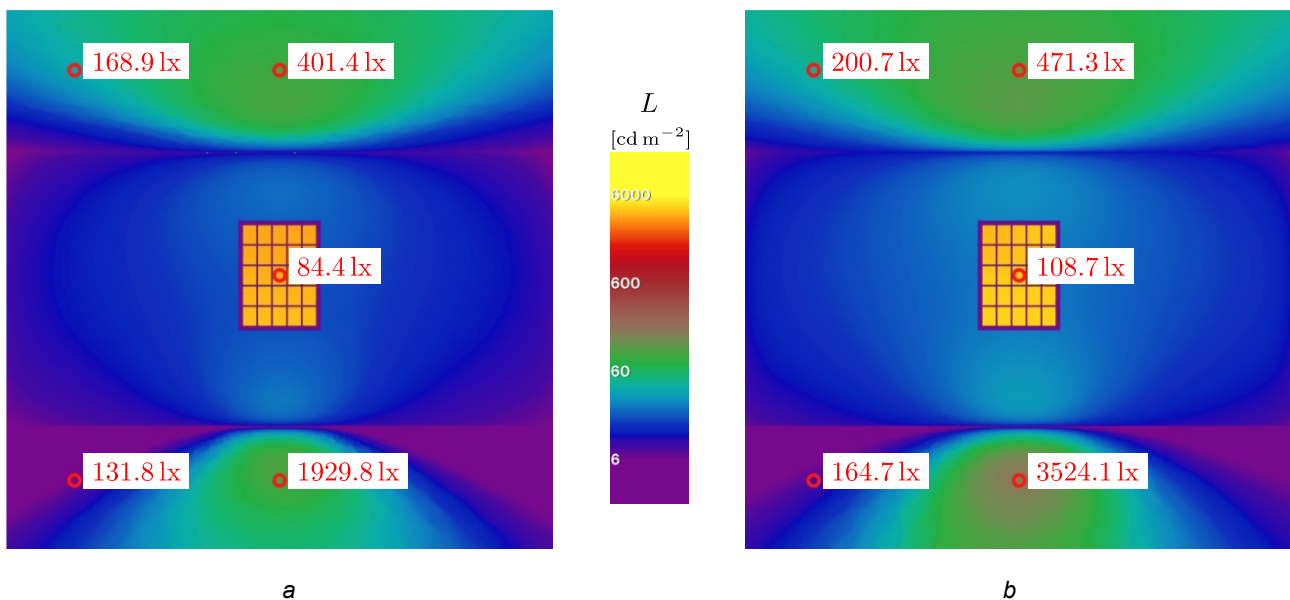
Fig. 11. Falsecolor maps of luminance distributions, window modelled from Model M (a) and Model C (b).

Data-driven models of the sample

The top row of Fig. 9 shows the distributions returned by the measurement-based *Model M*. Results for three incident directions are illustrated. a) and c) represent directions that were included in the model generation ($\theta_i = 20°$ and $40°$). Consequently, only effects of fitting RBFs and the final data-reduction are expected. While a) and c) correspond to the result of the measurement illustrated by Fig. 6, the top Fig. 9 b) is the result of interpolation between the two measured directions, and predicts the distribution for an incident direction that was not part of the measurement ($\theta_i = 30°$).

The distributions predicted by the computationally generated *Model C* are illustrated in the lower row of Fig. 9. Note that no interpolation was required in the model generation process, since ray-tracing was performed for any pair of incident and outgoing direction of the initial tensor before data-reduction.

Fig. 10 shows a photograph of the sample (a) compared to *Model M* (b) and *Model C* (c), applied to a flat polygon.

The plots, as well as the imagery produced by applying the BSDF models to the sample's macro-geometry, show good overall agreement between the two data-driven scattering representations, and in a comparison between measurement or photography. As expected, local deviations of the sample from its average BSDF are not accounted for. Since the light scatter measurement as well as the modelling based on the surface's height maps did not resolve colour channels, results are photometric, not colorimetric.

Exemplary daylight simulation

The exemplary simulation of a view towards the South window provides the imagery comprising Fig. 11, based on measurement-based *Model M* (a) and computed *Model C* (b). Four types of surfaces (window panes, floor, ceiling, wall) can be distinguished in the analysis, that receive daylight by different mechanisms. Local values of illuminance (E) are overlaid on top of the colour-encoded luminance maps (L).

Both data-driven models predict scattering of the incident sunlight that causes the window panes to light up, with luminance reaching $L \approx 5,500$ cd/m^2 through the glass panes. Illuminance on the inner side of the window is only due to inter-reflection from distant, opaque surfaces and therefore low with $E \approx 84$ lx for *Model M*, and $E \approx 109$ lx for *Model C*.

The floor is predominantly illuminated by light that is directly transmitted downward. This corresponds to the peak in the measured BSDF, that was replicated by both models. Consequently, the two synthetic images both feature a pronounced, bright region of the floor. It is significantly brighter with *Model C*. The smooth boundaries of these brighter areas are due to forward scattering that is indicated by the width of the peak in measurement and both models. Illuminance reaches values of $E \approx 1,930$ lx and $\approx 3,524$ lx for *Model M* and *Model C* respectively. The illuminance falls off toward the sides, with similar illuminance values predicated by both models ($E \approx 132$ lx and ≈ 165 lx).

The diffuse background of the BSDF causes scattering toward the ceiling. While the luminance is higher than the floor's due to its reflectivity, the illuminance in the centre of the ceiling reaches 401 lx or 21 % of that on the floor for *Model M*, and 471 lx or 13 % for *Model C*. The result indicates that the measurement-based model predicts a higher degree of diffuse scattering than the computational model, and agrees with the higher directional forward scattering of the latter, reflected by a significantly higher illuminance on the floor in the directly illuminated central region.

The luminance distribution on the Lambertian wall, which is directly correlated to the illuminance on the vertical surface, shows good agreement for both models. Illuminance on the inside of the window is lower for *Model M*.

Conclusions and outlook

The examination of the glass finds revealed a pronounced structure, that resembles effects of corrosion processes. This structure covers the traces of the manufacturing process and thereby obfuscates its expected effect on the light scattering properties of late antique window glass. A method to eliminate the later deterioration from the characterisation of the glass properties is therefore needed to reconstruct its effect on the natural illumination of buildings.

Both modelling methods are applicable to represent the glass panes in their current state in RADI-ANCE. In an exemplary daylight simulation, both models agreed qualitatively, replicating all effects such as widened directional transmission, scattering from the illuminated glass toward the observer leading to an apparent glow of the panes, and the diffuse scattering of daylight. This agrees with the similar distributions predicted by the models for selected incident directions. The significant differences found by quantitative comparison of simulation results in terms of illuminance, which was performed for few selected positions in the image domain, revealed that computationally generated *Model C* predicts stronger directional scattering than *Model M*, based on direct BSDF measurements. It is concluded that the qualitative appearance of the glass can be sufficiently described by the computational model, which accounts only for scattering by the glass surfaces. However, to achieve quantitative agreement between both models, this is not sufficient. One possible explanation is by the impact of scattering by inclusions and bubbles in the glass, which is absent in *Model C*.

Based on this finding, only methods that account for the scattering by the glass mass are considered as viable to model the original light scattering properties of the window glass. Two modelling approaches are considered by the authors, and will be developed and tested in future research. The first relies on the direct measurement of light scattering, such as in the generation of *Model M*. However, rather than an archaeological find, replicated samples produced by the known manufacturing techniques would have to form the base of this approach to isolate the deterioration effects. The second approach employs ray-tracing on geometric models of the micro-structure, such as in the generation of *Model C*, but including the inclusions and bubbles that were not modelled in the presented research. The development of such geometric models could be guided by microscopy in analogy, but aim only at artefacts due to manufacturing rather than the direct translation of the scanned height map into a light scattering model.

Acknowledgements

References

Apian-Bennewitz, P. (2010). New scanning gonio-photometer for extended BRTF measurements, *Proceedings SPIE – Optical Engineering + Applications* 7792, San Diego, United States, 1st September 2010. SPIE. 77920O. doi: 10.1117/12.860889.

Apian-Bennewitz, P. (2014). Scanning gonio-photometers for asymmetric acquisition of fine-structured BSDF, *Proceedings of Eurographics Workshop on Material Appearance Modeling*, University Lyon 2, France. 25th–27th June 2014. The Eurographics Association. pp. 1–4. doi: 10.2312/mam.20141291.

Arletti, R. et al. (2010). 'Roman window glass: A comparison of findings from three different Italian sites'. *Archaeometry* 52(2), pp. 252–271. doi: 10.1111/j.1475-4754.2009.00479.x.

ASTM International (2019). *ASTM E 2387-19 Standard practice for goniometric optical scatter measurements*. West Conshohocken, PA, United States. ASTM International. doi: 10.1520/E2387-19.

Baatz, D. (1991). Fensterglastypen, Glasfenster und Architektur. *Bautechnik der Antike*. Diskussionen zur Archäologischen Bauforschung 5. German Archaeological Institute, Berlin, Germany 15th–17th February 1990. Philipp von Zabern, Mainz, Germany. pp. 4–13.

Dai, Q. et al. (2009). 'The dual-microfacet model for capturing thin transparent slabs', *Computer Graphics Forum*, 28. pp. 1917–1925. doi: 10.1111/j.1467-8659.2009.01570.x.

De Rousiers, C. et al. (2011). Real-time rough refraction, in *Proceedings of I3D'11: SIGGRAPH Symposium on Interactive 3D Graphics and Games*, Marriott Fisherman's Wharf, San Francisco, CA, United States, 18th–20th February 2011. ACM, New York, NY, United States, pp. 111–118. doi: 10.1145/1944745.1944764.

Degryse, P. et al. (2014). 'The archaeometry of ancient glassmaking: Reconstructing ancient technology and the trade of raw materials', *Perspective* 2. pp. 224–238. doi: 10.4000/perspective.5617.

Demetrescu, E. et al. (2016). 'Reconstructing the original splendour of the House of Caecilius Iucundus. A complete methodology for virtual archaeology aimed at digital exhibition', *SCIRES-IT* 6. pp- 51–66. doi: 10.2423/i22394303v6n1p51.

Devlin, K. (2012). 'Just how predictable is predictive lighting?', in Bentkowska-Kafel, A., Denard, H. and Baker D. (eds.) *Para-data and transparency in virtual heritage. Digital research in the arts and humanities.* Farnham, United Kingdom: Ashgate Publishing, pp. 125–134.

Earl, G. et al (2013). 'Formal and informal analysis of rendered space: The Basilica Portuense', in Bevan, A. and Lake, M. (eds.) *Computational approaches to archaeological spaces*. Walnut Creek, CA, United States: Left Coast Press, pp. 265–305.

Foy, D. and Fontaine, S. D. (2008). 'Diversité et évolution du vitrage de l'Antiquité et du haut Moyen Âge: Un état de la question', *Gallia* 65. pp. 405–459. doi: 10.3406/galia.2008.3349.

Geisler-Moroder, D. and Dür, A. (2010). 'A new Ward BRDF model with bounded albedo', *Computer Graphics Forum* 29. pp. 1391–1398. doi: 10.1111/j.1467-8659.2010.01735.x.

Grobe, L. O. et al. (2010). 'Das Licht in der Hagia Sophia – Eine Computersimulation', in Daim, F. and Drauschke, J. (eds.) *Byzanz – das Römerreich im Mittelalter.* Mainz, Germany: Römisch-Germanisches Zentralmuseum. pp. 97–111.

Grobe, L. O. and Noback, A. (2019). Light scattering by Roman window glass [Data-set]. doi: 10.5281/zenodo.3265014

Grobe, L. O. (2018). 'Characterization and data-driven modeling of a retro-reflective coating in Radiance', *Energy and Buildings* 162. pp. 121–133. doi: 10.1016/j.enbuild.2017.12.029.

Grobe, L. O. et al. (2019). 'Data-driven modelling of daylight scattering by Roman window glass', *Journal of Computing and Cultural Heritage* 13. doi: 10.1145/3350428.

Haevernick, T. E. (1981a). 'Römische Fensterscheiben', in Haevernick, T. E. *Beiträge zur Glasforschung. Die wichtigsten Aufsätze von 1938 bis 1981*. Mainz, Germany: Philipp von Zabern. pp. 24–27.

Haevernick, T. E. (1981b). 'Untersuchungen römischer Fenstergläser', in Haevernick, T. E. *Beiträge zur Glasforschung. Die wichtigsten Aufsätze von 1938 bis 1981*. Mainz, Germany: Philipp von Zabern. pp. 33–38.

Happa, J. et al. (2012). 'Cultural heritage predictive rendering', *Computer Graphics Forum* 31(6). pp. 1823–1836. doi: https://doi.org/10.1111/j.1467–8659.2012.02098.x.

Heckbert, P. S. (1991). *Simulating global illumination using adaptive meshing*. PhD. University of California, Berkeley, CA, United States.

Inanici, M. (2014). 'Lighting analysis of Hagia Sophia', *Annual of Hagia Sophia Museum* 17. Istanbul, Turkey, pp. 128–202.

Jones, N. L. and Reinhart, C. F. (2017). 'Experimental validation of ray tracing as a means of image-based visual discomfort prediction', *Building and Environment* 113. pp. 131–150. doi: 10.1016/j.buildenv.2016.08.023.

Kajiya, J. T. (1986). The rendering equation, *Proceeding of the 13th Annual Conference on Computer Graphics and Interactive Techniques*, Dallas Convention Center, Dallas, TX, 18th–22nd August 1986. ACM, New York, United States. pp. 143–150. doi: 10.1145/15922.15902.

Kanyak, S. (2009). 'Late Roman / early Byzantine window glass from the Marmaray rescue excavation at Sirkeci, Istanbul', in Laflı, E. (ed.) *Late Antique / Early Byzantine Glass in the Eastern Mediterranean*. Colloquia Anatolica et Aegaea. Acta Congressus Internationalis Smyrnensis 2. Izmir, Turkey: Dokuz Eylül Üniversitesi. pp. 25–47.

La Torre, M. (2008). 'VI.5 Fenster', in Steskal, M. and La Torre, M. (eds.) *Das Vediusgymnasium in Ephesos. Archäologie und Baubefund*. Forschungen in Ephesos 14(1). Vienna, Austria: Austrian Archaeological Institute. pp. 286–288.

Karlsson, J. and Roos, A. (2000). 'Modelling the angular behaviour of the total solar energy transmittance of windows', *Solar Energy* 69. pp. 321–329. doi: 10.1016/S0038-092X(00)00083-9.

Komp, J. (2009). *Römisches Fensterglas: Archäologische und archäometrische Untersuchungen zur Glasherstellung im Rheingebiet.* PhD. Universität Frankfurt, Frankfurt am Main, Germany.

Kuhn, T. E. (2017). 'State of the art of advanced solar control devices for buildings', *Solar Energy* 154. pp. 112–133. doi: 10.1016/j.solener.2016.12.044.

Ladstätter, S. (2019). Ephesos from Late Antiquity until the Middle Ages. An archaeological introduction, in Ladstätter S. and Magdalino, P. (eds.) *Ephesos from Late Antiquity until the Middle Ages. Proceedings of the International Conference at the Research Center for Anatolian Civilizations*, Koç University, Istanbul, Turkey, 30th November–2nd December 2012. Austrian Archaeological Institute, Vienna, Austria. pp. 11–72.

Mau, A. (1899). *Pompeii, its Life and Art*. New York, United States: Macmillan.

Michielin, L. (2019). *Fores et fenestrae. A computational study of doors and windows in Roman domestic space*. PhD. University of Edinburgh, Edinburgh, United Kingdom.

Lee, E. S. et al. (2018). 'Modeling the direct sun component in buildings using matrix algebraic approaches: Methods and validation', *Solar Energy* 160. pp. 380–395. doi: 10.1016/j.solener.2017.12.029.

Monteoliva, J. M. et al. (2019). Dynamic cubic illuminance: An example of application of new paradigm for daylight analysis in an ancient Pompeian domus, in Corrado, V. and Gasparella, A. (eds.) *Proceedings of Building Simulation 2019: 16th Conference of IBPSA*, Angelicum Congress Centre Rome, Italy, 2nd–4th September 2019. IBPSA.

Noback, A. et al. (2017). *Measuring and modelling scattering properties of Roman window glass for daylight simulation* [Poster presentation]. *Glass of the Caesars @ 30*. London, United Kingdom. doi: 10.13140/RG.2.2.11607.78240/1.

Noback, A. et al. (2018). *Modeling the effects of daylight scattering by window glass: The case of 6th century Hagia Sophia in Istanbul* [Presentation]. *21st Congress of the Association Internationale pour l'Histoire du Verre*. Istanbul, Turkey. doi: 10.5281/zenodo.1414007.

Noback, A. (2019). 'Lichtsimulation in der digitalen Rekonstruktion historischer Architektur', in Kuroczyński, P., Pfarr-Harfst, M. and Münster, S. (eds.) *Der Modelle Tugend 2.0*. Heidelberg, Germany: Universitätsbibliothek Heidelberg. pp. 162–185. doi: 10.11588/arthistoricum.515.

Ochoa, C. E. et al. (2012). 'State of the art in lighting simulation for building science: a literature review', *Journal of Building Performance Simulation* 5. pp. 209–233. doi: 10.1080/19401493.2011.558211.

Papadopoulos, C. and Earl, G. (2014). 'Formal three-dimensional computational analyses of archaeological spaces' in Paliou, E., Lieberwirth, U. and Polla, S. (eds.) *Spatial analysis and social spaces. Interdisciplinary approaches to the interpretation of prehistoric and historic built environments*. Berlin, Germany: De Gruyter. pp. 135–166.

Schintlmeister, L. (2018). Glas aus einem spätantik-mittelalterlichen Stadtquartier in Ephesos. Ein Zwischenbericht, in Meinecke, K. and Schorner, G. (eds.) *Akten des 16. Österreichischen Archäologentages am Institut für Klassische Archäologie der Universität Wien 2016. Wiener Forschungen zur Archäologie*. University of Vienna, Austria, 25th–27th February 2016. pp. 437–442.

Stover, J. C. (2012). *Optical scattering: Measurement and analysis*. Bellingham, WA, United States: SPIE Optical Engineering Press. doi: 10.1117/3.975276.

Von Saldern, A. (1980). 'Ancient and Byzantine glass from Sardis', in Von Saldern, A. *Archaeological exploration of Sardis*. Monograph 6. Cambridge, MA, United States: Harvard University Press.

Von Saldern, A. (2004). *Antikes Glas. Handbuch der Archäologie*. Munich, Germany: C. H. Beck.

Schwaiger, H. et al. (2020). A late antique city quarter in Ephesos: Social differentiation and functional heterogeneity, in Flohr, M. and Montieux, N. (eds.) *Shops, Workshops and Urban Economic History in the Roman World, Archaeology and Economy in the Ancient World – Proceedings of the 19*[th] *International Congress of Classical Archaeology*, Cologne / Bonn, Germany, 22nd–26th May 2018. doi: 10.11588/propylaeum.573.

Spinazzola, V. (1953). *Pompei alla luce degli scavi nuovi di Via dell'Abbondanza (Anni 1910–1923).* Rome, Italy: Libreria della Stato.

Walter, B. et al. (2007). Microfacet models for refraction through rough surfaces, in Kautz, J. and Pattanaik, S. (eds.) *Proceedings of the 18*[th] *Eurographics conference on Rendering Techniques*, University of Grenoble, France, 25th–27th June 2007. Eurographics Association. Aire-la-Ville, Switzerland. pp. 195–206.

Ward, G. et al. (2012). *A practical framework for sharing and rendering real-world bidirectional scattering distribution functions.* Berkeley, CA, United States: Lawrence Berkeley National Laboratories.

Ward, G. et al. (2014). Reducing anisotropic BSDF measurement to common practice. *Proceedings of Eurographics Workshop on Material Appearance Modeling*, University Lyon 2, France. 25th–27th June 2014. Eurographics Association, Goslar, Germany. pp. 5–8. doi: 10.2312/mam.20141292.